

Bacterial Adhesion to Graphene Oxide (GO)-Functionalized Interfaces Is Determined by Hydrophobicity and GO Sheet Spatial Orientation

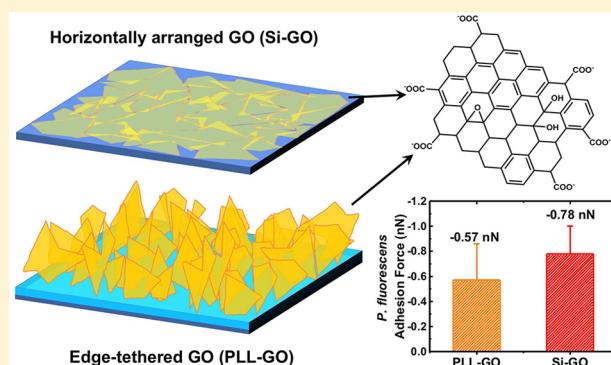
Jinkai Xue,^{*,†,‡} Sara BinAhmed,^{†,‡} Zhaoxing Wang,[†] Nathan G. Karp,[†] Benjamin L. Stottrup,[‡] and Santiago Romero-Vargas Castrillón^{*,†,‡}

[†]Department of Civil, Environmental, and Geo-Engineering, University of Minnesota, Twin Cities, 500 Pillsbury Dr. SE, Minneapolis, Minnesota 55455, United States

[‡]Department of Physics, Augsburg University, Minneapolis, Minnesota 55454, United States

Supporting Information

ABSTRACT: The potential of graphene oxide (GO) in environmental applications, such as the development of antimicrobial materials and low-fouling membranes, has thus far been hindered by an incomplete understanding of bioadhesion mechanisms on GO interfaces. Using atomic force microscopy (AFM)-based single-cell force spectroscopy, we investigate the adhesion of single *Pseudomonas fluorescens* cells on GO-functionalized interfaces possessing distinct morphologies. Specifically, we investigate Si-GO surfaces, in which Langmuir–Blodgett GO films are transferred to Si wafers by dip-coating, forming an immobilized layer of horizontally arranged GO nanosheets, and PLL-GO surfaces, where GO nanosheets, edge-tethered to poly-L-lysine, form an interface characterized by morphological and conformational disorder. We observe strong adhesion forces on both Si-GO and PLL-GO surfaces; analysis of the pull-off forces in terms of the worm-like chain model reveals that adhesion is driven by hydrophobic interactions between proteinaceous adhesins on *P. fluorescens* and graphenic basal planes. We further show that adhesion forces are significantly stronger on Si-GO surfaces that facilitate interactions with graphenic planes, compared to PLL-GO surfaces, which show weaker adhesion due to steric and electrostatic repulsion. These results therefore demonstrate that the spatial orientation and conformational disorder of GO nanosheets are key factors governing the interfacial properties of graphene nanomaterials.



1. INTRODUCTION

The significant interest in graphene nanomaterials is motivated by their unique physical and chemical properties. Graphene is the thinnest, strongest material ever developed.¹ As a 2-D nanomaterial with metallic properties, it is finding applications in electronic and photovoltaic devices.² The high surface area and photocatalytic-enhancing properties of graphene hold promise in environmental remediation, adsorption, degradation of organic contaminants, and the development of water purification membranes.^{2,3} Furthermore, graphene and graphene oxide (GO) exhibit wide-spectrum antibacterial activity,^{4–9} opening new avenues for the development of biocidal materials and interfaces, such a low-biofouling membranes.^{10,11} Nonetheless, further deployment of graphene-based biocidal materials has been hindered by an incomplete understanding of the adhesion mechanisms of bacteria on graphenic interfaces. Previous studies have attempted to explain the interactions between cells and individual graphenic sheets in suspension, with contradictory conclusions documented by different investigators. Li et al.¹² and Tu et al.,¹³ using a combination of microscopy and

simulation, proposed that graphene^{12,13} and GO sheets¹³ pierce lipid bilayers via sheet asperities or edges; a mechanism for bilayer piercing was provided based on molecular dynamics simulation, which showed spontaneous piercing of the cell membrane when graphene and GO sheets translocate orthogonally to the cell.^{12,13} On the other hand, AFM-based force spectroscopy measurements showed that the interactions of a GO-coated AFM probe with *E. coli* cell membranes were predominantly repulsive, possibly due to negatively charged GO sheet edges, which result in electrostatic repulsive forces as the nanosheets impinge on the cell membrane edge-first.^{12,14} These studies suggest that GO sheet spatial orientation plays an important role in determining the behavior of interfaces functionalized with GO. The relevance of nanosheet configuration is underscored by reports that nanosheet edge-bacteria contact is a determinant of biocidal activity,^{9,15} with a recent

Received: November 12, 2017

Revised: December 7, 2017

Accepted: December 13, 2017

Published: December 13, 2017

study reporting higher biocidal activity in GO films comprising, edge-exposed, vertically aligned nanosheets,¹⁶ though this view remains contentious.^{17–19} Nonetheless, direct, real-time experimental measurements examining the adhesion forces of bacteria on GO surfaces and the possible role played by GO sheet orientation in GO-cell adhesion forces are still lacking. In this work, we use atomic force microscopy (AFM)-based force spectroscopy to quantitatively evaluate the interactions of single *P. fluorescens* cells, a biofilm forming,^{20,21} environmentally relevant bacterium found in soil and drinking water,^{22,23} with substrates possessing horizontally oriented or randomly oriented GO surface coatings. We find strong bacterial adhesion on GO-functionalized surfaces, driven by hydrophobic interactions between proteinaceous adhesins and graphenic basal planes in GO. Further, we demonstrate that *P. fluorescens* adhesion is stronger on “flat” GO surface coatings as compared to randomly oriented surface coatings, demonstrating the importance of spatial orientation of GO as a design variable in GO surface coatings.

2. MATERIALS AND METHODS

2.1. Preparation of GO and GO Model Surfaces.

GO was prepared following a modification of Hummers' method, as explained in the Supporting Information (SI).²⁴ Confocal Raman spectroscopy, AFM, and scanning electron microscopy (SEM) were performed to characterize the GO sheets. The characteristic D ($\sim 1350\text{ cm}^{-1}$) and G ($\sim 1590\text{ cm}^{-1}$) bands²⁵ of GO were identified in the Raman spectrum (Figure S1(a)). GO sheets showed an average sheet size (Figure S1(b)) of $\sim 0.08\ \mu\text{m}$ (SEM images were analyzed with Fiji²⁶) and sheet thickness (Figure S1(c, d)) of $\sim 1\text{ nm}$, in agreement with previous reports.¹⁴ Zeta potential measurements of GO in aqueous dispersion (Figure S1(e)) showed that the nanosheets are negatively charged, due to deprotonation of carboxylic acid groups at the sheet edges.^{27,28}

Two model GO surfaces (i.e., randomly oriented GO sheets and horizontally oriented GO sheets) were prepared. The first class (denoted as PLL-GO surfaces) was prepared by covalently tethering GO sheets to poly-L-lysine (PLL)-coated glass (Poly-Prep slides, Sigma-Aldrich) via amine coupling chemistry.²⁹ The second class of surfaces (designated Si-GO) was prepared by transferring a GO Langmuir–Blodgett (LB) film¹⁷ to a P-type silicon (Si) wafer via dip-coating.³⁰ Details on the preparation of GO surfaces can be found in the SI. GO immobilized on the PLL-GO and Si-GO surfaces was confirmed by Raman spectroscopy. Surface roughness, hydrophobicity, and zeta potential were evaluated using AFM, captive bubble contact angle, and streaming current measurements, respectively, as described in the SI.

2.2. AFM-Based Single Cell Force Spectroscopy.

Pseudomonas fluorescens ATCC 13525 was used in all single-cell force spectroscopy (SCFS) experiments. As in other bacteria of the *Pseudomonas* genus, *P. fluorescens* has high bioadhesion and biofilm formation potential, owing to an array of adhesins,³¹ including flagella, pili, lipopolysaccharides (LPS), and outer membrane proteins (OMP) that influence its motility and adhesiveness.^{32–35} Single *P. fluorescens* cells were adhered to the cantilever using a polydopamine (PDA) wet adhesive.^{36,37} Details of the bacterial growth conditions and preparation of bacterial cell AFM probes are given in our recent publication³⁸ and summarized in the SI.

An MFP-3D-Bio AFM (Asylum Research) integrated to a Zeiss Axio Observer A.1 inverted optical microscope was used

for single-cell force measurements at room temperature ($25\text{ }^\circ\text{C}$). Extension–retraction cycles were performed at a cantilever speed of 400 nm/s , force distance of $2\ \mu\text{m}$ (longer force distances were used whenever long-range interactions were observed), and trigger force of 600 pN . Force curves were acquired at randomly chosen sites on the specimen surface; only three replicate force curves were recorded over each site to minimize deposition of extracellular polymeric substances. For each model surface, at least three individual cells (from three independent cell cultures) were used to collect a total of ≈ 100 curves. Raw data (i.e., cantilever deflection versus piezo Z position) were converted into force–separation curves, recording from each pull-off curve the maximum adhesion force (F_{Ad}) and rupture separation (L_{R}) (i.e., the separation at which surface forces vanish). Cell viability was checked after each experiment by a live/dead assay (BaClight). Only data collected with a live cell that remained at its initial location (such as that shown in Figure S12) are reported and discussed.

3. RESULTS AND DISCUSSION

3.1. Characterization of the Surfaces. Raman spectroscopy maps and AFM topographic images (collected in PBS buffer, pH 7.4) of the GO surfaces are provided in Figure 1.

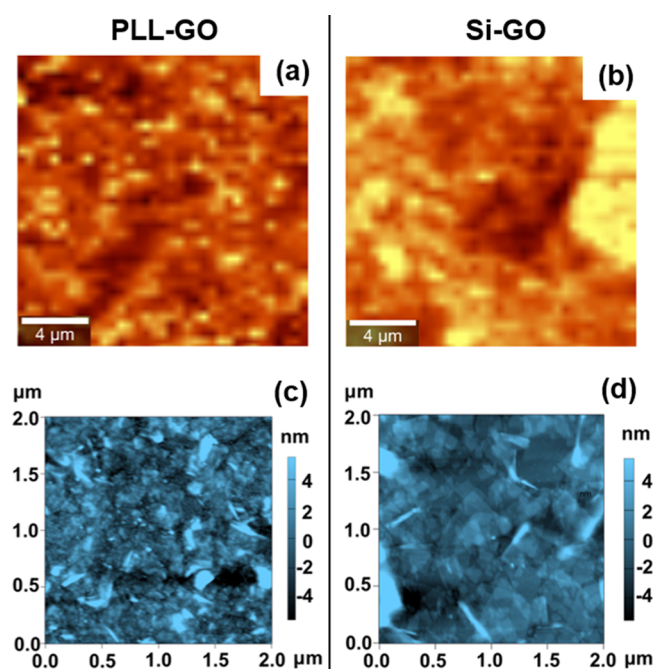


Figure 1. Surface characterization of PLL-GO (left column) and Si-GO surfaces (right column). (a, b) Raman spectroscopy maps of PLL-GO (a) and Si-GO (b) substrates. (c, d) Tapping mode AFM images of PLL-GO (c) and Si-GO (d) substrates. AFM imaging was conducted in PBS buffer, pH 7.4.

The Raman maps (Figure 1(a, b) and Figure S3(a, b)) show regions of high brightness (proportional to the intensity of the D and G peaks of GO), albeit with dissimilar spatial distribution: small (typically $< 1\ \mu\text{m}$) regions of high brightness were observed on the PLL-GO surface (Figure 1(a)), whereas the Si-GO surface exhibited larger GO domains ($\geq 1\ \mu\text{m}$), suggesting the presence of horizontally arranged GO (Figure 1(b)). In control surfaces (GO-free PLL and Si), Raman intensity is significantly attenuated (Figures S3(c, d)). The morphological features of Figure 1(a, b) are consistent with the

AFM images (Figure 1(c, d)), showing that two different spatial orientations are realized by these surfaces: GO nanosheets on Si-GO surfaces are stacked horizontally on the Si substrate (Figure 1(d) and Figure S2(b)), whereas a significantly more disordered interface is obtained when GO is tethered to flexible PLL chains (cf. PLL-GO, Figure 1(c) and Figure S2(a)), where horizontally oriented sheets on the substrate are not observed. In accord with the morphological features described in Figure 1, the root-mean-square roughness (R_{RMS} , Figure S4(a)) of PLL-GO ($R_{\text{RMS}} = 2.78$ nm) is higher than that of Si-GO ($R_{\text{RMS}} = 1.62$ nm, which suggests a GO film 1–2 sheets thick on Si). Figure S4(a) further shows that the presence of GO increases the roughness of the unmodified control substrates (note the lower surface roughness of bare PLL and Si surfaces). The orientational disorder of GO nanosheets in PLL-GO is partially due to the roughness of the underlying PLL, and it is also a consequence of bonding GO to primary amines in PLL, which allows edge-tethered solvated nanosheets to undergo thermal agitation. The zeta potential values showed that the four surfaces were negatively charged, exhibiting similar surface potentials (–60 to –90 mV) at pH 7.4 (Figure S4(b)).

The wettability of the surfaces, characterized by the contact angle of captive *n*-decane droplets in PBS (pH 7.4), is presented in Figure S5. Low contact angles (i.e., low *n*-decane wettability) are observed in all surfaces; H-bonding functional groups present in PLL (primary amine groups) and PLL-GO (epoxide, hydroxyl, and carboxylic groups that decorate the GO sheet edges^{27,39}) explain the poor wettability with *n*-decane. The similarity of contact angle values observed in Si and Si-GO is consistent with the wetting translucency⁴⁰ of graphene films. Given its ultrathin-sheet geometry, a significant fraction of the *n*-decane-Si van der Waals interactions are transmitted through the graphenic planes, resulting in wetting behavior that is relatively unaffected by the graphene coating.^{41,42}

3.2. GO Nanosheet Spatial Orientation and Hydrophobicity Are Determining Factors of Bacterial Adhesion. Figure 2(a) presents the mean maximum adhesion force ($\langle F_{\text{Ad}} \rangle$, where F_{Ad} is defined in the inset) observed on control and GO surfaces; adhesion force histograms for each system are given in Figure S6. GO functionalization has a significant effect on cell adhesion, as shown by the doubling of $\langle F_{\text{Ad}} \rangle$ in PLL-GO compared to PLL substrates and the order-of-magnitude increase in $\langle F_{\text{Ad}} \rangle$ observed in Si-GO surfaces compared to the Si control. The mean adhesion forces presented in Figure 2(a) increase as Si (–0.01 nN) < PLL (–0.28 nN) < PLL-GO (–0.57 nN) < Si-GO (–0.78 nN) ($p < 0.01$ from two-sided unpaired *t*-tests); these reflect cell–substrate adhesion forces, as demonstrated by the significantly weaker forces observed in control measurements with bacterium-free PDA-coated cantilevers (Figure S7, $p < 0.01$ except Si, on which weak adhesions are observed with and without cell). To explain the results shown in Figure 2(a), we note that bacterial adhesion is determined by a variety of cell–surface structures, such as pili and outer membrane proteins,^{34,35,43} which, owing to the high content of hydrophobic amino acids (in e.g., pilin proteins⁴⁵), mediate attachment to hydrophobic substrates via hydrophobic interactions.^{44,45} At the micro- and nanoscales both PLL-GO and Si-GO surfaces present hydrophobic regions embedded in the graphenic planes of the nanosheets,^{27,46} which are known to serve as adsorption sites for hydrophobic molecules.^{27,47–49} Consequently, the significant increase in $\langle F_{\text{Ad}} \rangle$ observed over Si-GO and PLL-GO is ascribed to hydrophobic association of cell–surface adhesins with hydrophobic domains in GO sheets.

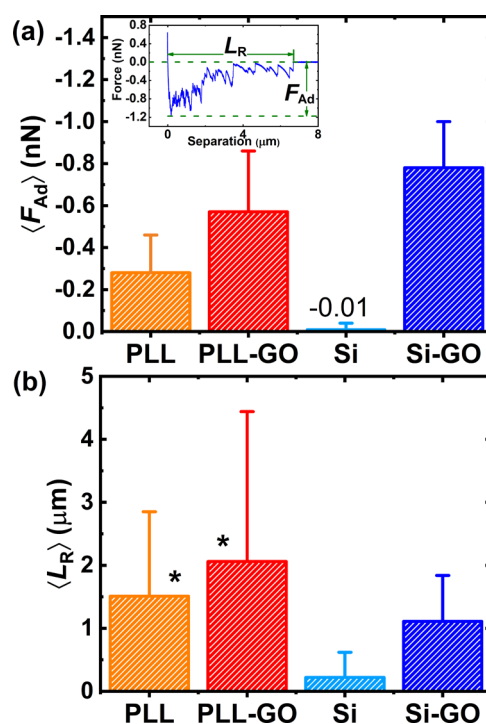


Figure 2. Results of single-cell force spectroscopy. (a) Average maximum adhesion force ($\langle F_{\text{Ad}} \rangle$) of *P. fluorescens* cells on the various surfaces. A representative pull-off force curve showing the definition of F_{Ad} and L_{R} is shown in the inset of panel (a). (b) Mean rupture separation ($\langle L_{\text{R}} \rangle$, the separation at which adhesion forces vanish). All experiments were performed in PBS buffer (pH 7.4). The histograms from which the reported means were computed are given in Figures S6 and S8; $p < 0.01$ (two-tailed unpaired *t*-test) for all pairwise comparisons except when indicated by *.

The determining role of hydrophobicity in *P. fluorescens* attachment is underscored by the weak adhesion (~ 10 pN, cf. Figure 2(a)) observed on Si substrates, the most hydrophilic surface investigated in this work (cf. Figure S5). Furthermore, we observe stronger ($p < 0.01$) $\langle F_{\text{Ad}} \rangle$ over Si-GO than PLL-GO (–0.78 nN vs –0.57 nN, respectively, cf. Figure 2(a)). The different adhesiveness demonstrated by PLL-GO and Si-GO is derived from their respective morphologies. Si-GO surfaces, as shown in Figure 1(d), exhibit horizontally arranged GO sheets, whereas GO sheets tethered to PLL form a rougher and more disordered PLL-GO interface (Figure 1(c) and Figure S4(a)). The flat GO sheet orientation in Si-GO surfaces therefore maximizes the surface area of graphenic planes with which cell biopolymers interact, thereby facilitating bacterial attachment. Low roughness of Si-GO (Figure S4(a)) may also enable bacterial attachment, as observed with pyrolytic graphite.¹⁵ Conversely, bacteria adhering on PLL-GO face negatively charged GO sheet edges,²⁸ which weaken bacterial attachment due to electrostatic repulsive forces.¹⁴ In addition, GO sheets edge-tethered to PLL create a steric barrier against microbial deposition, akin to that formed by solvated polymers.^{50–52} As a bacterium adheres on PLL-GO, GO nanosheets are compressed, the resulting loss of conformational entropy opposing cell adhesion.⁵⁰ These data thus demonstrate that nanosheet spatial arrangement (i.e., flat vs randomly oriented) and conformational degrees of freedom play key roles in determining the GO–bacterial cell adhesion forces.

To gain insight into the cell–surface structures mediating adhesion, we analyzed the rupture distance (L_{R}), defined in

Figure 2(a) (inset). The values of the mean rupture distance ($\langle L_R \rangle$) are presented in Figure 2(b), and the distributions of L_R appear in Figure S8. Apart from the Si control, over which no significant adhesion is observed, mean L_R values reported by PLL, PLL-GO, and Si-GO surfaces (1–2 μm) are consistent with bioadhesion mediated by membrane proteins (contour length $\approx 2 \mu\text{m}$ ^{34,35}); a fraction of measurements showing $L_R > 2 \mu\text{m}$ (Figure S8 for PLL, PLL-GO, and Si-GO) is likely due to pili-mediated adhesion, which can extend to several micrometers.^{53,54} Long L_R values may also be attributed to stretching of PLL chains on the glass substrates, as shown by the longer-ranged forces exhibited by PLL and PLL-GO compared to Si-GO substrates (Figure 2(b)).

3.3. Proteinaceous Adhesins Mediate *P. fluorescens* Attachment to GO-Functionalized Interfaces. In a subset ($\sim 20\%$) of the pull-off force–separation profiles recorded on PLL, PLL-GO, and Si-GO, we observed the sawtooth pattern (Figure 3(a)) that is associated with force unfolding of protein domains.^{44,55} As shown in the inset of Figure 3(a), the peaks are well fitted by the worm-like chain (WLC) model of polymer elasticity^{56,57} which describes the force F necessary to unravel a random coil as $F(x) = k_B T / L_p [0.25(1 - x/L_C)^{-2} + x/L_C -$

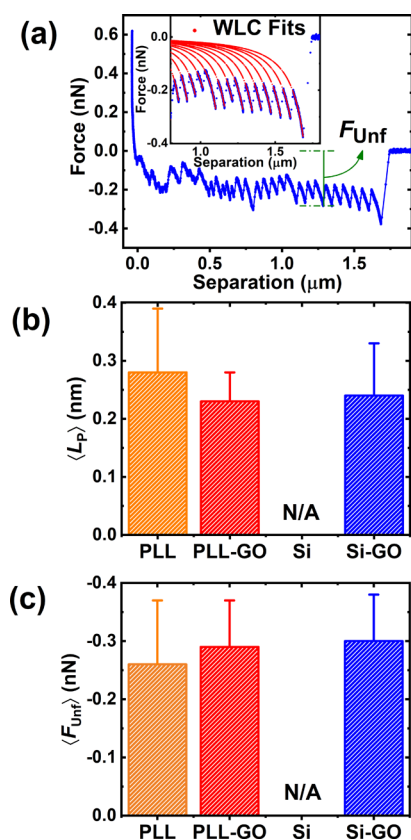


Figure 3. Signatures of macromolecular unfolding observed over different model surfaces. (a) Representative force curve exhibiting the sawtooth pattern characteristic of force-unfolding of macromolecular domains. Representative fits of the worm-like chain (WLC) model to the sawtooth patterns are shown in the inset. (b) Mean persistence length ($\langle L_p \rangle$) obtained from WLC model fits to the pull-off force curve of single *P. fluorescens* cells. (c) Mean unfolding force ($\langle F_{Unf} \rangle$). The definition of F_{Unf} is shown in panel (a). The histograms from which the means in panels (b) and (c) were computed are given in Figures S9 and S10. N/A for Si indicates that no signatures of macromolecular unfolding were observed on this substrate.

0.25], where x is separation, k_B is the Boltzmann constant, T is the absolute temperature (298 K), L_p is the persistence length (a measure of polymer rigidity), and L_C is the contour length (the length of the unfolded macromolecule). Quantitative analysis of the pull-off force curves in terms of the WLC model yielded values of L_p and L_C (in fitting the WLC model, we discarded nonspecific adhesion peaks at short separation, as well as peaks yielding $L_p < 0.15 \text{ nm}$, the length of a C–C bond⁵⁸). We find that best-fit L_p values were narrowly distributed with means in the 0.23–0.28 nm range (Figure 3(b) and Figure S9), close to the persistence length of proteins ($\sim 0.4\text{--}1 \text{ nm}$ ^{34,55,59,60}), and observed that the mean peak force (F_{Unf} , defined in Figure 3(a)) was consistent with the unfolding force of membrane proteins ($\sim 300 \text{ pN}$, cf. Figure 3(c) and Figure S10).^{34,55} The values of L_p and F_{Unf} suggest that adhesion of *P. fluorescens* is mediated by proteinaceous hydrophobic adhesins, likely to be membrane proteins that interact with hydrophobic graphenic planes in GO nanosheets, and lysyl side chains in PLL. The hydrophobic character of adhesin proteins is manifested by the absence of the sawtooth pattern in all force curves recorded over hydrophilic Si substrates. ΔL_C , the difference in contour lengths between consecutive sawtooth peaks, revealed the length scale of the unfolded domains. As shown in Figures S11(b, c), ΔL_C values for PLL-GO and Si-GO were distributed around means of 66.4 and 80.6 nm, respectively, which suggest that each sawtooth peak is due to unfolding of more than one protein domain (whose repeats are $\sim 30\text{--}40 \text{ nm}$ for membrane proteins³⁵ and $\sim 50\text{--}60 \text{ nm}$ in pilin proteins⁵³). The broader distribution of ΔL_C observed over PLL (Figure S11(a)) suggests that adhesins undergo surface-induced unfolding over this substrate.³⁴

In closing, we have demonstrated that the hydrophobic interactions that drive *P. fluorescens* adhesion are stronger in GO interfaces assembled from horizontally arranged nanosheets, as compared to edge-tethered GO sheets where electrostatic and steric repulsion weaken adhesion forces. Our results emphasize the importance of nanosheet hydrophobicity, spatial arrangement, and conformational disorder in determining the interfacial behavior of GO-functionalized substrates, pointing out possible directions for future inquiry. Reactive oxygen species (ROS)-mediated cell oxidation^{6,14} is likely to modify cell bioadhesion due to breakdown of the outer membrane. Experiments isolating the competing effect of ROS pose interesting questions that warrant future investigations. Further investigations should also aim to elucidate the mechanism of adhesion of hydrophilic bacteria⁶¹ to graphenic surfaces, perhaps using adhesin-knockout mutants.

■ ASSOCIATED CONTENT

📄 Supporting Information

The Supporting Information is available free of charge on the ACS Publications website at DOI: 10.1021/acs.estlett.7b00509.

Further information on materials and methods (GO synthesis and characterization, preparation and characterization of PLL-GO and Si-GO surfaces, and functionalization of AFM probes with bacterial cells). Results of GO characterization (Figure S1); AFM imaging, Raman spectroscopy images, AFM surface roughness, zeta potential, and contact angle measurements for all surfaces (Figures S2–S5); histograms of adhesion forces (Figures S6 and S7), rupture separations (Figure S8), persistence lengths (Figure S9), unfolding forces (Figure

S10), contour lengths (Figure S11); and digital image of bacterial cell AFM probe (Figure S12). (PDF)

AUTHOR INFORMATION

Corresponding Authors

*E-mail: xuexx145@umn.edu. Tel: +1 (226) 505-0458 (Jinkai Xue).

*E-mail: sromerov@umn.edu. Tel: +1 (612) 301-1347 (Santiago Romero-Vargas Castrillón).

ORCID

Santiago Romero-Vargas Castrillón: 0000-0003-3339-7692

Author Contributions

♦J. X. and S. BA. were equal contributors to this work.

Notes

The authors declare no competing financial interest.

ACKNOWLEDGMENTS

This work was supported by grants to S.R.-V.C. from the United States Geological Survey (MN WRC 2015MN362B), 3M Co. (Non-Tenured Faculty Award), and the Environment and Natural Resources Trust Fund, as recommended by the Legislative-Citizen Commission on Minnesota Resources. Portions of this work were carried out in the Characterization Facility and Minnesota Nano Center, University of Minnesota, which receive partial support from NSF through the MRSEC and NNIN programs, respectively. Work at Augsburg University was supported by NSF MRI 1040126.

REFERENCES

- (1) Lee, C.; Wei, X.; Kysar, J. W.; Hone, J. Measurement of the elastic properties and intrinsic strength of monolayer graphene. *Science (Washington, DC, U. S.)* **2008**, *321* (5887), 385–388.
- (2) Zhu, Y.; Murali, S.; Cai, W.; Li, X.; Suk, J. W.; Potts, J. R.; Ruoff, R. S. Graphene and graphene oxide: Synthesis, properties, and applications. *Adv. Mater.* **2010**, *22* (35), 3906–3924.
- (3) Hu, M.; Mi, B. Enabling graphene oxide nanosheets as water separation membranes. *Environ. Sci. Technol.* **2013**, *47* (8), 3715–3723.
- (4) Chen, J.; Peng, H.; Wang, X.; Shao, F.; Yuan, Z.; Han, H. Graphene oxide exhibits broad-spectrum antimicrobial activity against bacterial phytopathogens and fungal conidia by intertwining and membrane perturbation. *Nanoscale* **2014**, *6* (3), 1879–1889.
- (5) Hu, W.; Peng, C.; Luo, W.; Lv, M.; Li, X.; Li, D.; Huang, Q.; Fan, C. Graphene-based antibacterial paper. *ACS Nano* **2010**, *4* (7), 4317–4323.
- (6) Perreault, F.; De Faria, A. F.; Nejati, S.; Elimelech, M. Antimicrobial properties of graphene oxide nanosheets: Why size matters. *ACS Nano* **2015**, *9* (7), 7226–7236.
- (7) Gurunathan, S.; Han, J. W.; Dayem, A. A.; Eppakayala, V.; Kim, J. H. Oxidative stress-mediated antibacterial activity of graphene oxide and reduced graphene oxide in *Pseudomonas aeruginosa*. *Int. J. Nanomed.* **2012**, *7*, 5901–5914.
- (8) Chen, J.; Wang, X.; Han, H. A new function of graphene oxide emerges: Inactivating phytopathogenic bacterium. *J. Nanopart. Res.* **2013**, *15* (5), 1–14.
- (9) Akhavan, O.; Ghaderi, E. Toxicity of graphene and graphene oxide nanowalls against bacteria. *ACS Nano* **2010**, *4* (10), 5731–5736.
- (10) Soroush, A.; Ma, W.; Cyr, M.; Rahaman, M. S.; Asadishad, B.; Tufenkji, N. In situ silver decoration on graphene oxide-treated thin film composite forward osmosis membranes: Biocidal properties and regeneration potential. *Environ. Sci. Technol. Lett.* **2016**, *3* (1), 13–18.
- (11) Perreault, F.; Jaramillo, H.; Xie, M.; Ude, M.; Nghiem, L. D.; Elimelech, M. Biofouling mitigation in forward osmosis using graphene oxide functionalized thin-film composite membranes. *Environ. Sci. Technol.* **2016**, *50* (11), 5840–5848.

(12) Li, Y.; Yuan, H.; von dem Bussche, A.; Creighton, M.; Hurt, R. H.; Kane, A. B.; Gao, H. Graphene microsheets enter cells through spontaneous membrane penetration at edge asperities and corner sites. *Proc. Natl. Acad. Sci. U. S. A.* **2013**, *110* (30), 12295–12300.

(13) Tu, Y.; Lv, M.; Xiu, P.; Huynh, T.; Zhang, M.; Castelli, M.; Liu, Z.; Huang, Q.; Fan, C.; Fang, H.; et al. Destructive extraction of phospholipids from *Escherichia coli* membranes by graphene nanosheets. *Nat. Nanotechnol.* **2013**, *8* (8), 594–601.

(14) Romero-Vargas Castrillón, S.; Perreault, F.; De Faria, A. F.; Elimelech, M. Interaction of graphene oxide with bacterial cell membranes: Insights from force spectroscopy. *Environ. Sci. Technol. Lett.* **2015**, *2* (4), 112–117.

(15) Pham, V. T. H.; Truong, V. K.; Quinn, M. D. J.; Notley, S. M.; Guo, Y.; Baulin, V. A.; Al Kobaisi, M.; Crawford, R. J.; Ivanova, E. P. Graphene induces formation of pores that kill spherical and rod-shaped bacteria. *ACS Nano* **2015**, *9* (8), 8458–8467.

(16) Lu, X.; Feng, X.; Werber, J. R.; Chu, C.; Zucker, I.; Kim, J.-H.; Osuji, C. O.; Elimelech, M. Enhanced antibacterial activity through the controlled alignment of graphene oxide nanosheets. *Proc. Natl. Acad. Sci. U. S. A.* **2017**, *114*, E9793.

(17) Mangadla, J. D.; Santos, C. M.; Felipe, M. J. L.; de Leon, A. C. C.; Rodrigues, D. F.; Advincula, R. C. On the antibacterial mechanism of graphene oxide (GO) Langmuir–Blodgett films. *Chem. Commun.* **2015**, *51* (14), 2886–2889.

(18) Hui, L.; Piao, J. G.; Auletta, J.; Hu, K.; Zhu, Y.; Meyer, T.; Liu, H.; Yang, L. Availability of the basal planes of graphene oxide determines whether it is antibacterial. *ACS Appl. Mater. Interfaces* **2014**, *6* (15), 13183–13190.

(19) Zucker, I.; Werber, J. R.; Fishman, Z. S.; Hashmi, S. M.; Gabinet, U. R.; Lu, X.; Osuji, C. O.; Pfefferle, L. D.; Elimelech, M. Loss of phospholipid membrane integrity induced by two-dimensional nanomaterials. *Environ. Sci. Technol. Lett.* **2017**, *4* (10), 404–409.

(20) O'Toole, G. A.; Kolter, R. Initiation of biofilm formation in *Pseudomonas fluorescens* WCS365 proceeds via multiple, convergent signalling pathways: A genetic analysis. *Mol. Microbiol.* **1998**, *28* (3), 449–461.

(21) Spiers, A. J.; Rainey, P. B. The *Pseudomonas fluorescens* SBW25 wrinkly spreader biofilm requires attachment factor, cellulose fibre and LPS interactions to maintain strength and integrity. *Microbiology* **2005**, *151* (9), 2829–2839.

(22) Haas, D.; Défago, G. Biological control of soil-borne pathogens by fluorescent pseudomonads. *Nat. Rev. Microbiol.* **2005**, *3* (4), 307–319.

(23) Hardalo, C.; Edberg, S. C. *Pseudomonas aeruginosa*: assessment of risk from drinking water. *Crit. Rev. Microbiol.* **1997**, *23* (1), 47–75.

(24) Tung, V. C.; Allen, M. J.; Yang, Y.; Kaner, R. B. High-throughput solution processing of large-scale graphene. *Nat. Nanotechnol.* **2009**, *4* (1), 25–29.

(25) Kudin, K. N.; Ozbas, B.; Schniepp, H. C.; Prud'homme, R. K.; Aksay, I. A.; Car, R. Raman spectra of graphite oxide and functionalized graphene sheets. *Nano Lett.* **2008**, *8* (1), 36–41.

(26) Schindelin, J.; Arganda-Carreras, I.; Frise, E.; Kaynig, V.; Longair, M.; Pietzsch, T.; Preibisch, S.; Rueden, C.; Saalfeld, S.; Schmid, B.; et al. Fiji: an open-source platform for biological-image analysis. *Nat. Methods* **2012**, *9* (7), 676–682.

(27) Sanchez, V. C.; Jachak, A.; Hurt, R. H.; Kane, A. B. Biological interactions of graphene-family nanomaterials: An interdisciplinary review. *Chem. Res. Toxicol.* **2012**, *25*, 15–34.

(28) Li, D.; Müller, M. B.; Gilje, S.; Kaner, R. B.; Wallace, G. G. Processable aqueous dispersions of graphene nanosheets. *Nat. Nanotechnol.* **2008**, *3* (2), 101–105.

(29) Grabarek, Z.; Gergely, J. Zero-length crosslinking procedure with the use of active esters. *Anal. Biochem.* **1990**, *185* (1), 131–135.

(30) Cote, L. J.; Kim, F.; Huang, J. Langmuir–Blodgett assembly of graphite oxide single layers. *J. Am. Chem. Soc.* **2009**, *131* (3), 1043–1049.

(31) Tamber, S.; Hancock, R. E. W. The outer membranes of *Pseudomonas*. In *Pseudomonas*; Ramos, J. L., Ed.; Springer, 2004; pp 575–601.

- (32) Dasgupta, N.; Arora, S.; Ramphal, R. The flagellar system of *Pseudomonas aeruginosa*. In *Pseudomonas*; Ramos, J. L., Ed.; 2004; Springer, pp 675–698.
- (33) Tolker-Nielsen, T.; Molin, S. The biofilm lifestyle of *Pseudomonas*. In *Pseudomonas*; Ramos, J. L., Ed.; Springer, 2004; pp 547–571.
- (34) El-Kirat-Chatel, S.; Boyd, C. D.; O'Toole, G. A.; Dufrene, Y. F. Single-molecule analysis of *Pseudomonas fluorescens* footprints. *ACS Nano* **2014**, *8* (2), 1690–1698.
- (35) El-Kirat-Chatel, S.; Beaussart, A.; Boyd, C. D.; O'Toole, G. A.; Dufrene, Y. F. Single-cell and single-molecule analysis deciphers the localization, adhesion, and mechanics of the biofilm adhesin LapA. *ACS Chem. Biol.* **2014**, *9* (2), 485–494.
- (36) Lee, H.; Dellatore, S. M.; Miller, W. M.; Messersmith, P. B. Mussel-inspired surface chemistry for multifunctional coatings. *Science (Washington, DC, U. S.)* **2007**, *318* (5849), 426–430.
- (37) Kang, S.; Elimelech, M. Bioinspired single bacterial cell force spectroscopy. *Langmuir* **2009**, *25* (17), 9656–9659.
- (38) BinAhmed, S.; Hasane, A.; Wang, Z.; Mansurov, A.; Romero-Vargas Castrillón, S. Bacterial adhesion to ultrafiltration membranes: Role of hydrophilicity, natural organic matter, and cell-surface macromolecules. *Environ. Sci. Technol.* **2017**, DOI: 10.1021/acs.est.7b03682.
- (39) Park, S.; An, J.; Jung, I.; Piner, R. D.; An, S. J.; Li, X.; Velamakanni, A.; Ruoff, R. S. Colloidal suspensions of highly reduced graphene oxide in a wide variety of organic solvents. *Nano Lett.* **2009**, *9* (4), 1593–1597.
- (40) Rafiee, J.; Mi, X.; Gullapalli, H.; Thomas, A. V.; Yavari, F.; Shi, Y.; Ajayan, P. M.; Koratkar, N. A. Wetting transparency of graphene. *Nat. Mater.* **2012**, *11* (3), 217–222.
- (41) Shih, C.-J.; Strano, M. S.; Blankschtein, D. Wetting translucency of graphene. *Nat. Mater.* **2013**, *12* (10), 866–869.
- (42) Shih, C. J.; Wang, Q. H.; Lin, S.; Park, K. C.; Jin, Z.; Strano, M. S.; Blankschtein, D. Breakdown in the wetting transparency of graphene. *Phys. Rev. Lett.* **2012**, *109* (17), 176101.
- (43) Vesper, S. J. Production of pili (fimbriae) by *Pseudomonas fluorescens* and correlation with attachment to corn roots. *Appl. Environ. Microbiol.* **1987**, *53* (7), 1397–1405.
- (44) Dufrene, Y. F. Sticky microbes: Forces in microbial cell adhesion. *Trends Microbiol.* **2015**, *23*, 376–382.
- (45) Ong, Y. L.; Razatos, A.; Georgiou, G.; Sharma, M. M. Adhesion forces between *E. coli* bacteria and biomaterial surfaces. *Langmuir* **1999**, *15* (8), 2719–2725.
- (46) Erickson, K.; Erni, R.; Lee, Z.; Alem, N.; Gannett, W.; Zettl, A. Determination of the local chemical structure of graphene oxide and reduced graphene oxide. *Adv. Mater.* **2010**, *22* (40), 4467–4472.
- (47) Cote, L. J.; Kim, J.; Tung, V. C.; Luo, J.; Kim, F.; Huang, J. Graphene oxide as surfactant sheets. *Pure Appl. Chem.* **2010**, *83* (1), 95–110.
- (48) Kim, J.; Cote, L. J.; Kim, F.; Yuan, W.; Shull, K. R.; Huang, J. Graphene oxide sheets at interfaces. *J. Am. Chem. Soc.* **2010**, *132* (23), 8180–8186.
- (49) Liu, Z.; Robinson, J. T.; Sun, X.; Dai, H. PEGylated nanographene oxide for delivery of water-insoluble cancer drugs. *J. Am. Chem. Soc.* **2008**, *130* (33), 10876–10877.
- (50) Prime, K. L.; Whitesides, G. M. Adsorption of proteins onto surfaces containing end-attached oligo(ethylene oxide): A model system using self-assembled monolayers. *J. Am. Chem. Soc.* **1993**, *115* (23), 10714–10721.
- (51) Prime, K.; Whitesides, G. Self-assembled organic monolayers: model systems for studying adsorption of proteins at surfaces. *Science (Washington, DC, U. S.)* **1991**, *252* (5009), 1164–1167.
- (52) Gon, S.; Kumar, K. N.; Nüsslein, K.; Santore, M. M. How bacteria adhere to brushy PEG surfaces: Clinging to flaws and compressing the brush. *Macromolecules* **2012**, *45* (20), 8373–8381.
- (53) Filloux, A.; de Bentzmann, S.; Aurouze, M.; Lazdunski, A.; Vallet, I. Fimbrial genes in *Pseudomonas aeruginosa* and *Pseudomonas putida*. In *Pseudomonas*; Ramos, J. L., Ed.; Springer, 2004; pp 721–748.
- (54) Whitechurch, C. B. Biogenesis and function of type IV pili in *Pseudomonas* species. In *Pseudomonas*; Ramos, J. L., Ed.; Springer, 2006; pp 139–188.
- (55) Rief, M.; Gautel, M.; Oesterhelt, F.; Fernandez, J. M.; Gaub, H. E. Reversible unfolding of individual titin immunoglobulin domains by AFM. *Science (Washington, DC, U. S.)* **1997**, *276* (5315), 1109–1112.
- (56) Bustamante, C.; Marko, J.; Siggia, E.; Smith, S. Entropic elasticity of lambda-phage DNA. *Science (Washington, DC, U. S.)* **1994**, *265* (5178), 1599–1600.
- (57) Israelachvili, J. N. *Intermolecular and Surface Forces*, Third ed., Academic Press, 2011.
- (58) Abu-Lail, N. I.; Camesano, T. A. Elasticity of *Pseudomonas putida* KT2442 surface polymers probed with single-molecule force microscopy. *Langmuir* **2002**, *18* (10), 4071–4081.
- (59) Walther, K. A.; Grater, F.; Dougan, L.; Badilla, C. L.; Berne, B. J.; Fernandez, J. M. Signatures of hydrophobic collapse in extended proteins captured with force spectroscopy. *Proc. Natl. Acad. Sci. U. S. A.* **2007**, *104* (19), 7916–7921.
- (60) Stirnemann, G.; Giganti, D.; Fernandez, J. M.; Berne, B. J. Elasticity, structure, and relaxation of extended proteins under force. *Proc. Natl. Acad. Sci. U. S. A.* **2013**, *110* (10), 3847–3852.
- (61) Krasowska, A.; Sigler, K. How microorganisms use hydrophobicity and what does this mean for human needs? *Front. Cell. Infect. Microbiol.* **2014**, *4*, 1–7.

Supporting Information

Bacterial Adhesion to Graphene Oxide (GO)-Functionalized Interfaces is Determined by Hydrophobicity and GO Sheet Spatial Orientation

Jinkai Xue^{1,*}♦, Sara BinAhmed¹♦, Zhaoxing Wang¹, Nathan G. Karp¹, Benjamin L. Stottrup², Santiago Romero-Vargas Castrillón^{1,*}

Environ. Sci. Technol. Lett.

¹ Department of Civil, Environmental, and Geo- Engineering, University of Minnesota, Twin Cities, Minneapolis, MN 55455, USA

² Department of Physics, Augsburg University, Minneapolis, MN 55454

♦J. X. and S. BA. were equal contributors to this work

Contents: 17 pages and 12 figures

*Corresponding authors: Jinkai Xue. Email: xuexx145@umn.edu. Tel: +1 (226) 505-0458. Santiago Romero-Vargas Castrillón. Email: sromerov@umn.edu. Tel: +1 (612) 301-1347.

Supporting Materials and Methods

Synthesis of GO

Graphene oxide (GO) was prepared *via* chemical exfoliation of graphite (Bay Carbon, SP-1, 325 mesh) using a modified Hummers method.¹ First, 2.0 g of graphite was placed in 5 mL of concentrated sulfuric acid at 80 °C. Next, 2.0 g each of K₂S₂O₈ and P₂O₅ were added and the suspension was allowed to react at 80 °C for 4.5 hours. After reaction, the mixture was transferred into 320 mL of ultrapure water (18.2 MΩ cm, Barnstead, Thermo Fisher) and allowed to settle overnight. The mixture was subsequently vacuum filtered using PTFE membranes (0.45 μm, Whatman TE 36) and dried overnight at room temperature. Next, the obtained black solid was mixed with 80 mL of concentrated sulfuric acid over an ice bath, and 10.0 g of KMnO₄ was slowly added so that the temperature of the mixture did not exceed 10 °C. The mixture was then slowly heated to 35 °C over a period of 2.5 hours. Next, 154 mL of ultrapure water was slowly added, preventing the suspension temperature from exceeding 50 °C, and reacted for 2 hours at room temperature. Lastly, the mixture was transferred to 480 mL of ultrapure water, and 8.4 mL of 30% H₂O₂ was added, causing the mixture to acquire a yellowish-brown color. The suspension was allowed to settle for 2 days, and the precipitate was subsequently recovered by multiple centrifugation steps (12,000 × g, 30 min), initially re-suspending the product in 10% HCl to remove chemical residues and finishing with resuspension in water until the supernatant reached a pH of about 3.5. Finally, the suspended product was purified *via* dialysis (3.5 kDa membranes, Spectrum Labs) for 4 days and lyophilized for 4 days.

Preparation of PLL-GO Surfaces

GO sheets were covalently tethered to poly-L-lysine (PLL, MW = 150-300 kDa) immobilized on glass surfaces (Poly-Prep slides, Sigma Aldrich) *via* amine coupling² mediated by EDC (1-ethyl-3-(3-dimethylaminopropyl)carbodiimide hydrochloride) and NHS (*N*-hydroxysuccinimide), following established protocols.^{2,3} MES buffer (2-(*N*-morpholino)ethanesulfonic acid, 100 mM, pH 6.0) was mixed with GO aqueous dispersion (250 μg L⁻¹) at a 1:5 volume ratio. Next, EDC (20 mM) and NHS (50 mM) solutions prepared in 10 mM MES buffer were sequentially mixed with the GO suspension. During this step, carboxylic acid groups in GO are converted to amine-reactive esters. The reaction proceeded for 15 min at pH ~5.5. The pH of the suspension was subsequently adjusted to ~7.2 before immersing in the suspension a PLL-coated glass coupon. The suspension was placed on a shaker table (~30 rpm) for 1 h, after which the coupon was rinsed with ultrapure water, and bath-sonicated for ~10 min to remove unbound GO sheets. Prepared PLL-GO coupons were stored in ultrapure water at 4 °C until use.

Preparation of Si-GO Surfaces

Si-GO substrates were prepared *via* dip coating of Langmuir-Blodgett (LB) GO films on P-type silicon wafers (100 orientation, single side polished, test grade, 500- μm thickness). The bare silicon substrate was first soaked in acetone for 15 min, rinsed with copious amounts of ultrapure water, and washed with isopropyl alcohol to eliminate water residues. After air drying, the wafer was placed in a UV/O₃ cleaner for 20 min to eliminate organic residues (ProCleaner™ Plus, Bioforce Nanosciences). The cleaned wafer was stored in a nitrogen-purged desiccator before use.

The LB trough (effective area = 172 cm²) was cleaned with Alconox solution followed by thorough rinsing with ultrapure water. Thereafter the trough was filled with a sublayer consisting of HCl solution, pH 1.0. The Si wafer was then dipped vertically into the trough well with the upper end clamped on the dipper. Surface pressure was monitored using a Wilhelmy plate positioned parallel to the Si substrate. A mixture of GO dispersion (2 mg mL⁻¹) and methanol (v/v = 1/5) was added to the acidic water sublayer dropwise in 0.5-mL aliquots to a total of 2.5 mL. Five min was allowed between aliquot additions. The setup was left overnight for methanol to completely evaporate. Finally, the Si substrate was pulled up at a constant speed of 0.03 mm/s with a surface pressure of 5 mN/m. More information on GO LB film preparation is documented elsewhere.⁴⁻⁶

Confocal Raman Microscopy

Confocal Raman Microscopy (Witec Alpha300R) was performed in the study to confirm the two characteristic bands of GO materials and GO coverage on the model surfaces. Sample surfaces were scanned using a Nikon 100 \times objective, 532-nm laser excitation and 1800 grooves/mm grating.

The optimal depth for mapping was determined by performing an x-z scan over a 20 \times 8 μm^2 (length \times depth) cross-section. Next, the x-y Raman map was generated over a 20 \times 20 μm^2 scan area at the determined depth, with a resolution of 1 μm . Two spectra were measured per micron. The sum of the area under the D and G peaks of GO (found at $\sim 1350\text{ cm}^{-1}$ and $\sim 1590\text{ cm}^{-1}$, respectively⁷) was used to generate the signal intensity maps.

AFM Topography and Surface Roughness

An MFP-3D-Bio atomic force microscope (Asylum Research) was used to image the surfaces and measure their nanoscale roughness using tapping (AC) mode AFM in phosphate buffered saline (PBS, pH 7.4). Bruker SNL probes were used (cantilever C, nominal $k = 0.24\text{ N/m}$). Surface images were collected at 0.5 Hz over areas of 20 \times 20 μm^2 , 5 \times 5 μm^2 , and 2 \times 2 μm^2 , on each surface type. Root-mean-square (RMS) roughness was calculated from three randomly selected spots (0.5 $\mu\text{m} \times 0.5\text{ }\mu\text{m}$) on each surface type.

Contact Angle Goniometry

Contact angle measurements were performed with a Model 200 contact angle goniometer (Ramé-Hart) equipped with a fluid cell for captive bubble measurements. *n*-Decane drops (2 μ L) were injected into the fluid cell (filled with PBS, pH 7.4) and deposited on the surface using a syringe fitted with a J-shaped needle (Type 304 stainless steel, 22 gauge). The left and right contact angles were recorded after 60 s from digital images using the DROImage Standard software (Ramé-Hart). For each surface, 4 replicate specimens were measured for a total of \sim 10 deposited droplets.

Surface Charge (ζ -Potential)

The ζ -potential of the surfaces was determined from streaming current measurements using an electrokinetic analyzer (SurPASS, Anton Paar). Two 10×20 mm² specimen coupons were attached to sample holders using double-sided tape; sample holders were subsequently mounted in an adjustable gap cell, setting the gap size to \approx 110 μ m. The streaming current was measured by flowing the electrolyte solution (1 mM KCl) through the gap (i.e., parallel to the specimen coupons) as the pressure difference was increased to 400 mbar. A linear dependence of the streaming current with the pressure difference was observed, in accordance with the Helmholtz-Smoluchowski equation,⁸ and the ζ -potential was determined from the slope. Streaming potential measurements were performed at pH \sim 5.5 – 10 adding aliquots of 0.05 M NaOH. Two independently prepared samples of each surface type were characterized.

Bacterial Culture Conditions

The as-received freeze-dried bacterial culture powder (*P. fluorescens* ATCC 13525) was used to inoculate 6 mL of LB broth (Miller, Sigma-Aldrich). Following incubation for 2 hours at 30 °C, agar plates were streaked and incubated at 30 °C overnight to grow bacterial colonies. Bacterial suspensions were prepared by transferring a colony with a pipette tip to 50 mL of LB medium. The suspension was incubated overnight at 30 °C and 125 RPM shaking speed, and diluted (1:25) with fresh LB broth. After further incubation for \sim 3 hours at 30 °C and 175 RPM, cells were harvested in mid-exponential phase ($OD_{600\text{ nm}} \approx 0.4 - 0.6$), centrifuged at $5000 \times g$ for 1 min, and re-suspended in PBS, pH 7.4. This step was repeated thrice. All materials and reagents used in cell culture were autoclaved before use.

Sample Preparation and Cantilever Functionalization

A specimen of sample surface with a dimension of $\sim 1 \times 0.5$ cm² was adhered using epoxy (3M Quick Set Epoxy Adhesive) to a piranha- and UV/O₃-cleaned 35-mm circular glass disc (Asylum Research). After a 15-min epoxy curing step, a 20- μ L droplet of bacterial suspension was placed on the glass disc beside the specimen. The droplet was let to stand for 30 min to permit bacterial deposition on the glass surface. Afterward, 4 mL of PBS was used to rinse off excess unattached cells, avoiding contact between the specimen surface and the bacterial suspension. The glass disc

was mounted in the AFM fluid cell (Fluid Cell Lite, Asylum Research), which was then filled with 2 mL of PBS buffer (pH 7.4).

Tipless silicon nitride cantilevers with nominal $k = 0.01$ N/m (Bruker MLCT-O10 probe “C”) were used in force spectroscopy experiments. Cantilevers were cleaned in a UV/O₃ chamber for 25 min before use. A self-adherent polydopamine (PDA) coating^{9,10} was deposited on the AFM probe to enable attachment of a bacterial cell to the end of the cantilever. PDA deposition was conducted for 15 min (65 RPM shaking speed) from a solution containing 4 mg of dopamine hydrochloride (Sigma-Aldrich) per milliliter of Trizma buffer (10 mM, BioReagent, Sigma-Aldrich) buffered to pH 8.5. Following deposition, the probe was rinsed with ultrapure water and dried in a nitrogen-purged desiccator for 5 min. Prior to bacterial attachment, the cantilever optical lever sensitivity was measured over the bare glass surface, and the spring constant (k) was calibrated using the thermal noise method¹¹ (the values of k were within the range specified by the manufacturer). The AFM probe was mounted onto the AFM probe holder, and the AFM head was thereafter lowered into the fluid cell, allowing ~40 min for the cantilever deflection signal to reach a stable value. To prepare a single-cell AFM probe, the PDA-coated cantilever was engaged at a 1 nN loading force on a single bacterial cell identified using the 63× objective of the inverted optical microscope (Zeiss Axio Observer A.1). After 5 min, the cantilever (functionalized with the bacterial cell) was withdrawn.

Supporting Results

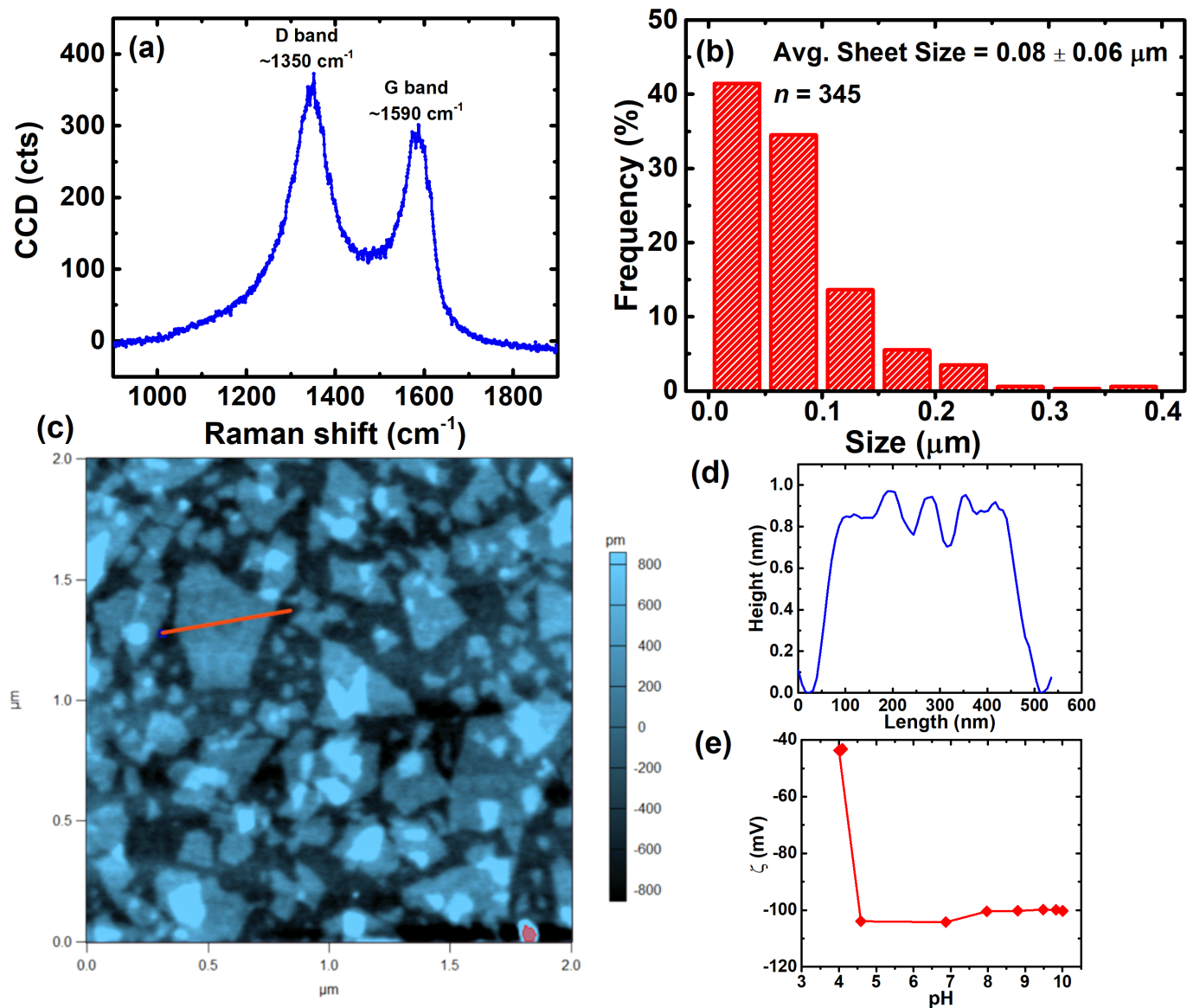


Figure S1: Characterization of graphene oxide (GO): (a) Raman spectrum; (b) sheet size (equivalent radius) distribution; (c) tapping mode AFM image of GO sheets deposited on silicon; (d) GO sheet height profile (determined along the red line in panel c); (e) zeta potential of GO in aqueous dispersion at a concentration of $250 \mu\text{g mL}^{-1}$.

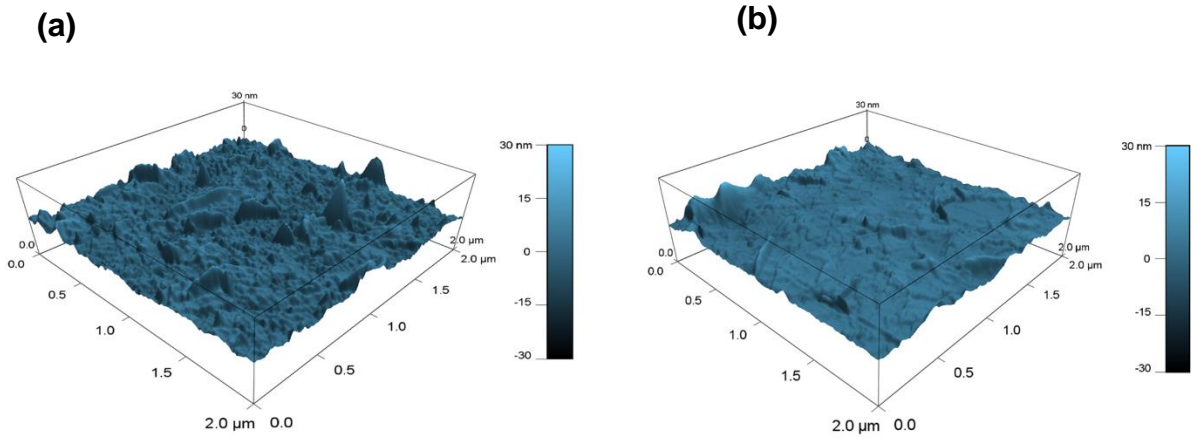


Figure S2: Surface topography visualized by tapping mode AFM: (a) PLL-GO and (b) Si-GO.

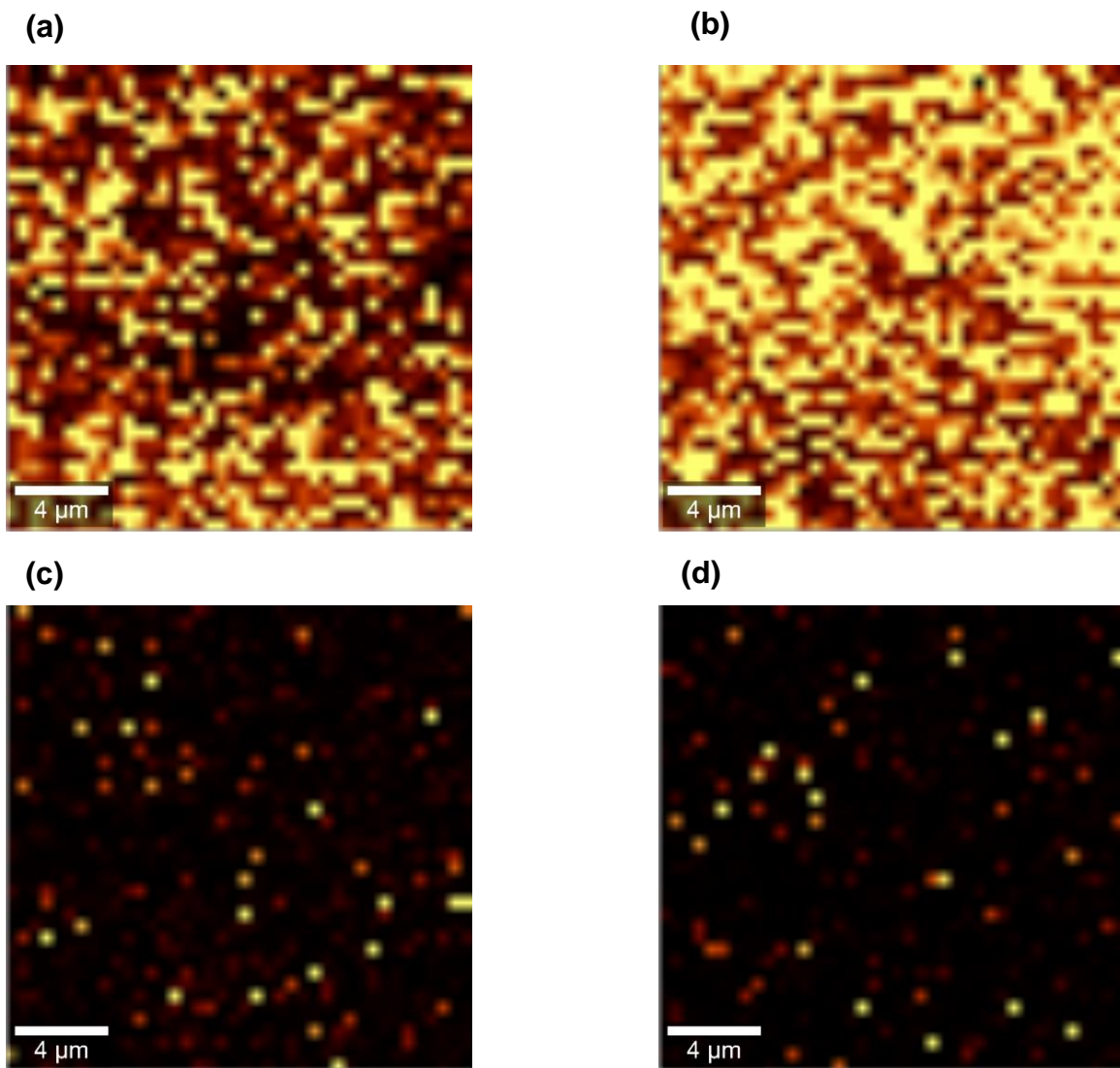


Figure S3: Raman spectroscopy images of (a) PLL-GO, (b) Si-GO, (c) PLL, and (d) Si surfaces.

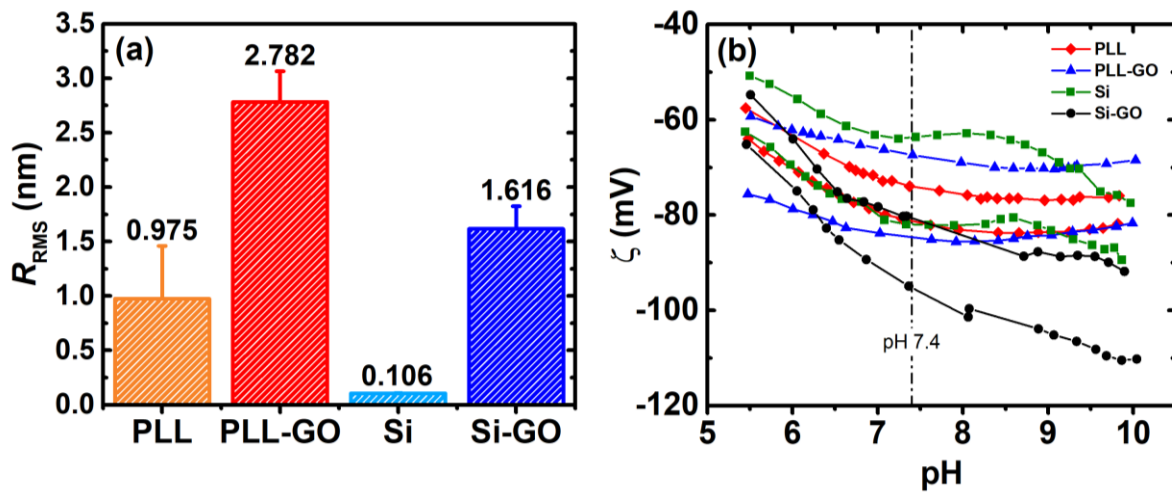


Figure S4: RMS roughness values (a) and ζ -potential as a function of pH (b) for the different surfaces.

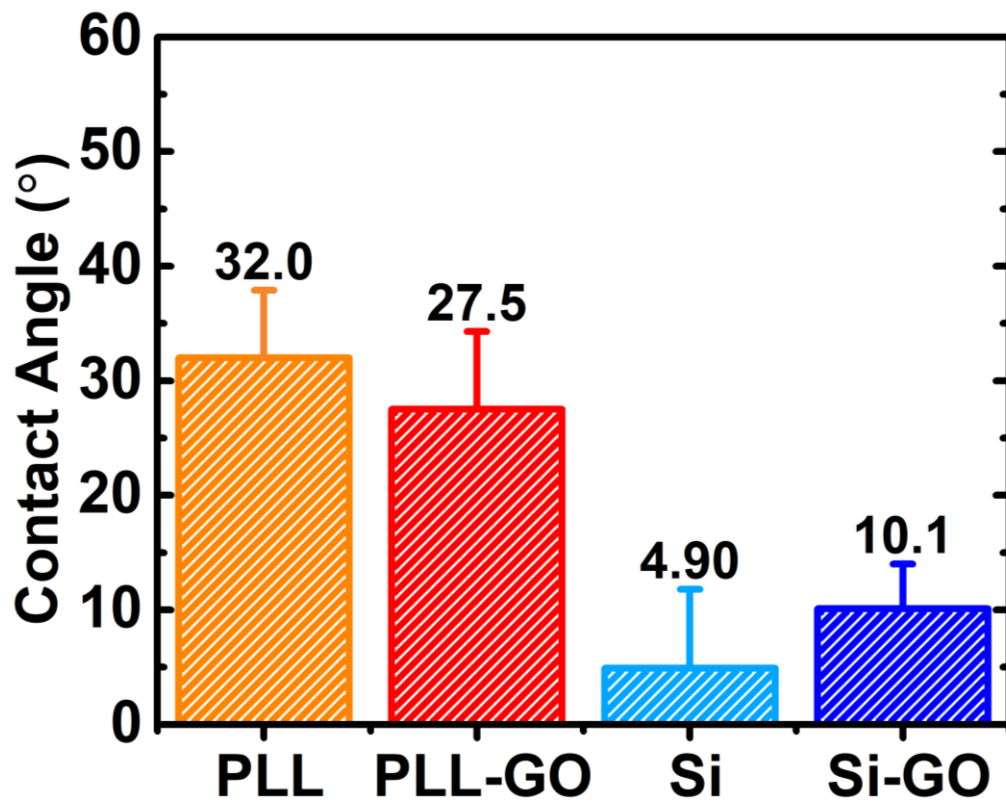


Figure S5: Contact angles obtained through the captive bubble method using *n*-decane droplets in PBS buffer (pH 7.4).

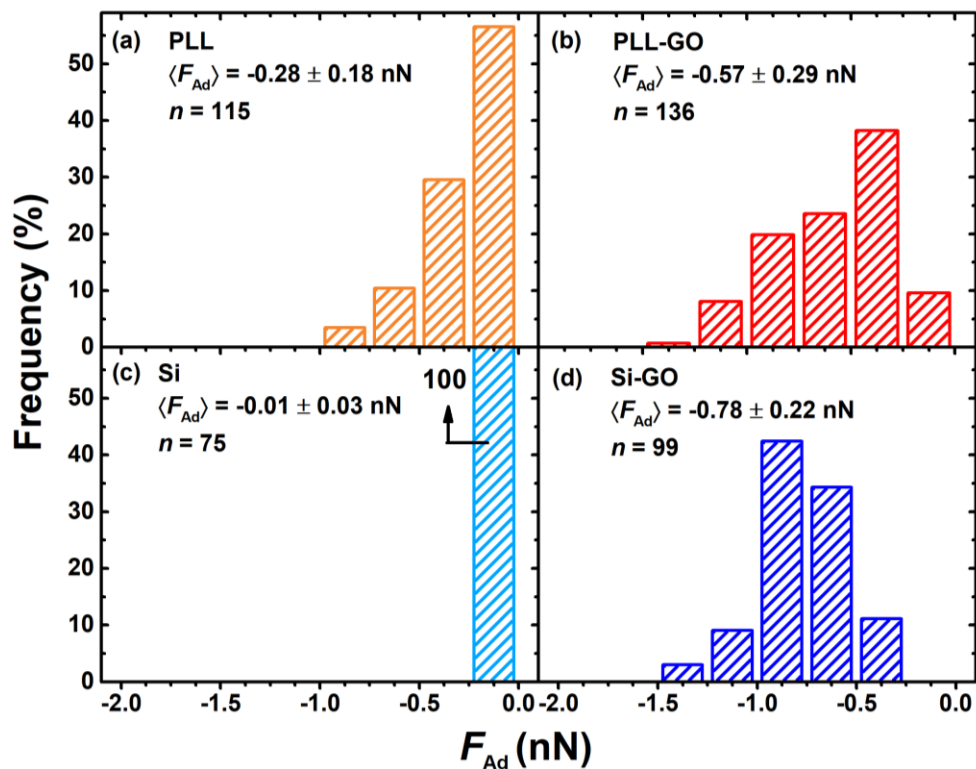


Figure S6: Distribution of maximum adhesion forces (F_{Ad}) of single *P. fluorescens* cells on: (a) poly-L-lysine-coated glass (PLL); (b) graphene oxide (GO)-functionalized PLL surfaces (PLL-GO); (c) Si wafers; (d) Langmuir-Blodgett GO films deposited on Si wafers by dip-coating (Si-GO). The inset shows the histogram average ($\langle F_{Ad} \rangle$), standard deviation, and number of measurements (n). Measurements were performed in PBS buffer (pH 7.4).

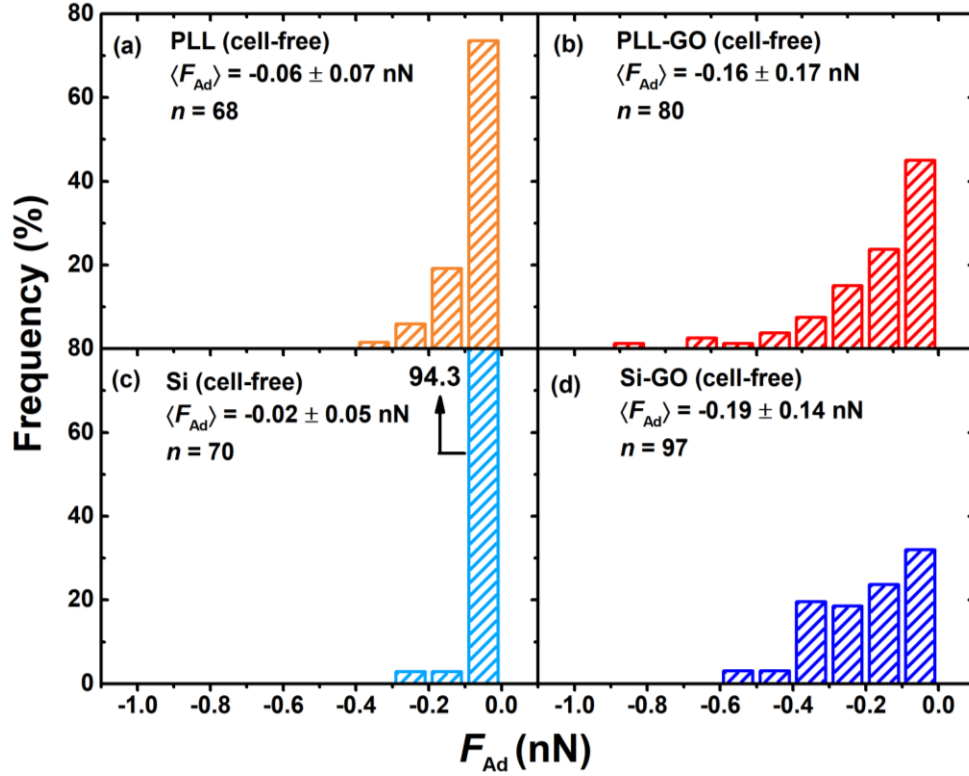


Figure S7: Distribution of maximum adhesion forces (F_{Ad}) of cell-free polydopamine-coated cantilevers on: (a) poly-L-lysine-coated glass (PLL); (b) graphene oxide (GO)-functionalized PLL surfaces (PLL-GO); (c) Si wafers; (d) Langmuir-Blodgett GO films deposited on Si wafers by dip-coating (Si-GO). The inset shows the histogram average ($\langle F_{Ad} \rangle$), standard deviation, and number of measurements (n). Experiments were performed in PBS buffer (pH 7.4).

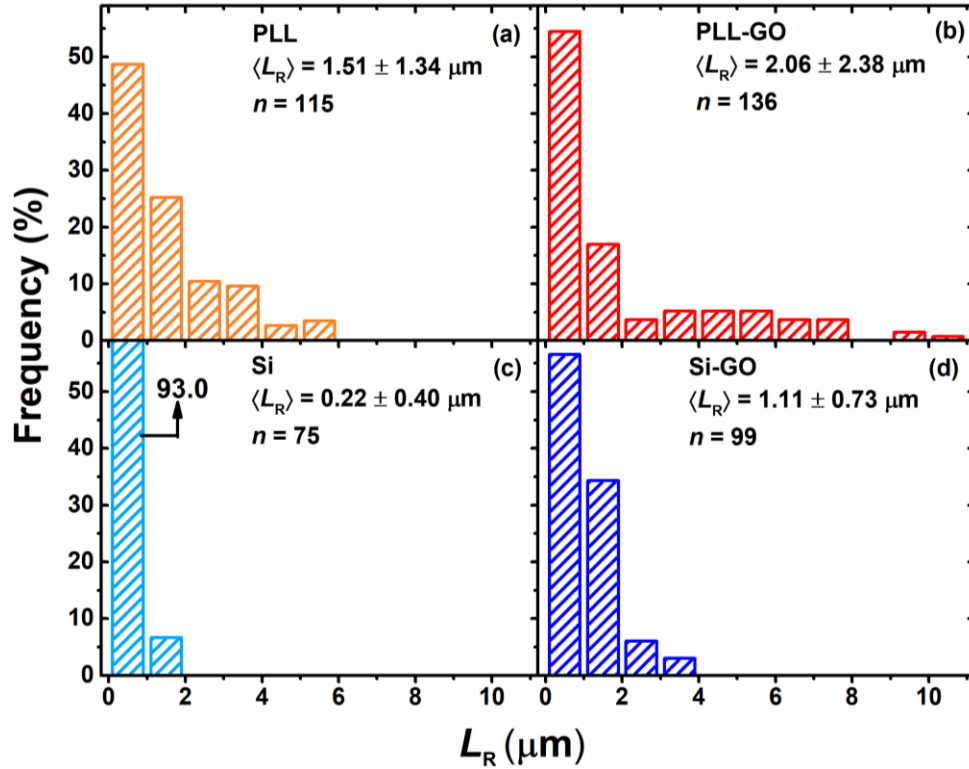


Figure S8: Distribution of rupture separation (L_R : distance from the surface at which adhesion forces vanish) for single *P. fluorescens* cells on: (a) poly-L-lysine-coated glass (PLL); (b) graphene oxide (GO)-functionalized PLL surfaces (PLL-GO); (c) Si wafers; (d) Langmuir-Blodgett GO films deposited on Si wafers by dip-coating (Si-GO). The inset shows the histogram average ($\langle L_R \rangle$), standard deviation, and number of measurements (n). Experiments were performed in PBS buffer (pH 7.4).

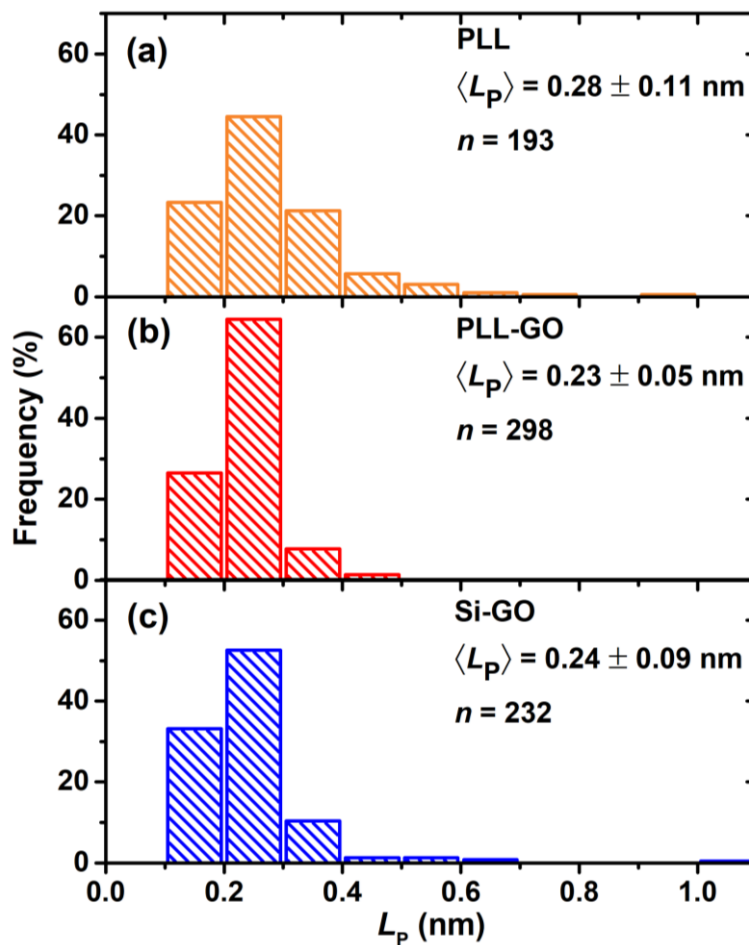


Figure S9: Distribution of best-fit persistence length values (L_p), obtained from WLC model fits to the pull-off force curve of single *P. fluorescens* cells on: (a) poly-L-lysine-coated glass (PLL); (b) graphene oxide (GO)-functionalized PLL surfaces (PLL-GO); (c) Langmuir-Blodgett GO films deposited on Si wafers by dip-coating (Si-GO). The inset shows the histogram average ($\langle L_p \rangle$), standard deviation, and number of measurements (n). Experiments were performed in PBS buffer (pH 7.4).

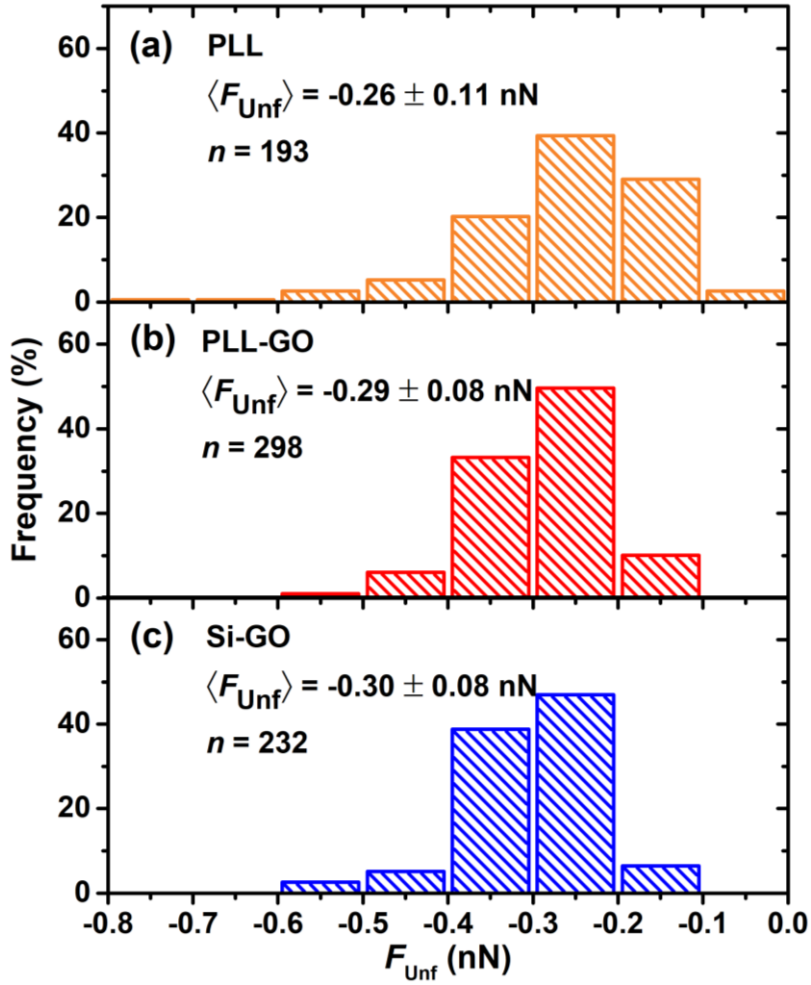


Figure S10: Distribution of the unfolding forces (F_{Unf} , the force measured at the sawtooth peak, cf. Figure 3(a)), obtained from the pull-off force curve of single *P. fluorescens* cells on: (a) poly-L-lysine-coated glass (PLL); (b) graphene oxide (GO)-functionalized PLL surfaces (PLL-GO); (c) Langmuir-Blodgett GO films deposited on Si wafers by dip-coating (Si-GO). The inset shows the histogram average ($\langle F_{\text{Unf}} \rangle$), standard deviation, and number of measurements (n). Experiments were performed in PBS buffer (pH 7.4).

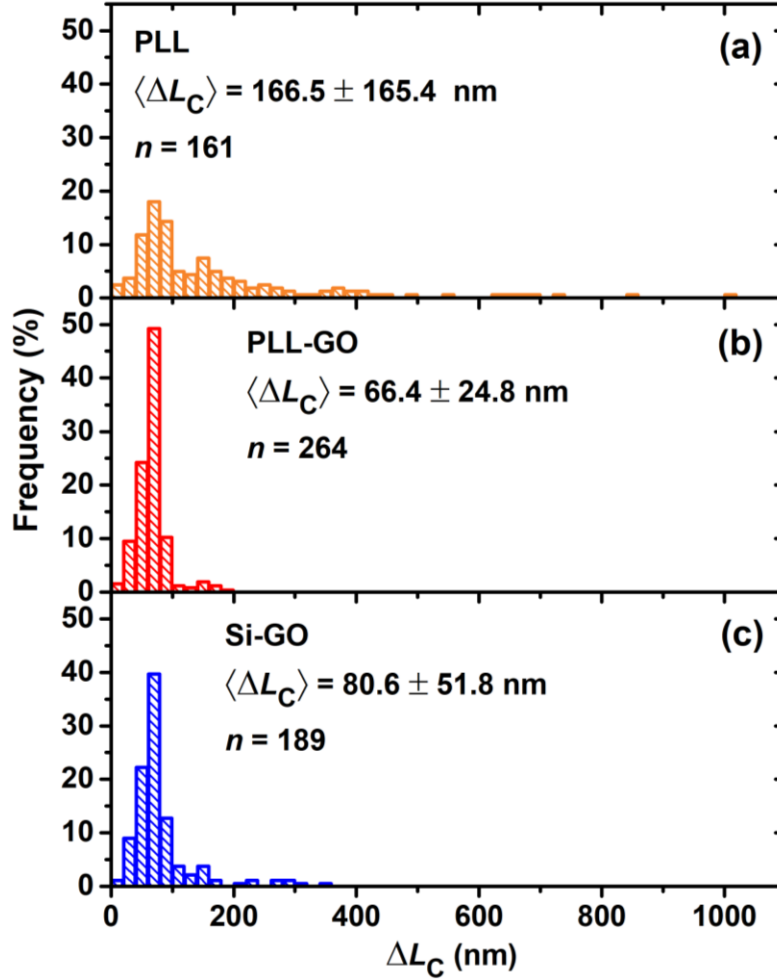


Figure S11: Distribution of ΔL_C (the difference in contour length between two consecutive sawtooth peaks), obtained from the pull-off force curve of single *P. fluorescens* cells on: (a) poly-L-lysine-coated glass (PLL); (b) graphene oxide (GO)-functionalized PLL surfaces (PLL-GO); (c) Langmuir-Blodgett GO films deposited on Si wafers by dip-coating (Si-GO). The inset shows the histogram average ($\langle \Delta L_C \rangle$), standard deviation, and number of measurements (n). Experiments were performed in PBS buffer (pH 7.4).



Figure S12: Bacterial cell probe imaged after force measurements. The bacterial cell (*P. fluorescens*) was attached to the front edge of a tipless AFM cantilever using polydopamine wet adhesive. The observed green fluorescence indicates that the cell remained viable throughout the experiment.

Supporting References

- (1) Tung, V. C.; Allen, M. J.; Yang, Y.; Kaner, R. B. High-throughput solution processing of large-scale graphene. *Nat. Nanotechnol.* **2009**, *4* (1), 25–29.
- (2) Grabarek, Z.; Gergely, J. Zero-length crosslinking procedure with the use of active esters. *Anal. Biochem.* **1990**, *185* (1), 131–135.
- (3) Hermanson, G. T. *Bioconjugate Techniques: Third Edition*; 2013, 259–266.
- (4) Valtierrez-Gaytan, C.; Ismail, I.; Macosko, C.; Stottrup, B. L. Interfacial activity of graphene oxide. *Colloids Surfaces A Physicochem. Eng. Asp.* **2017**, *529*, 434–442.
- (5) Cote, L. J.; Kim, F.; Huang, J. Langmuir-Blodgett assembly of graphite oxide single layers. *J. Am. Chem. Soc.* **2009**, *131* (3), 1043–1049.
- (6) Kim, F.; Cote, L. J.; Huang, J. Graphene oxide: Surface activity and two-dimensional assembly. *Adv. Mater.* **2010**, *22* (17), 1954–1958.
- (7) Kudin, K. N.; Ozbas, B.; Schniepp, H. C.; Prud'homme, R. K.; Aksay, I. A.; Car, R. Raman spectra of graphite oxide and functionalized graphene sheets. *Nano Lett.* **2008**, *8* (1), 36–41.
- (8) Werner, C.; Körber, H.; Zimmermann, R.; Dukhin, S.; Jacobasch, H. Extended electrokinetic characterization of flat solid surfaces. *J. Colloid Interface Sci.* **1998**, *208* (1), 329–346.
- (9) Lee, H.; Dellatore, S. M.; Miller, W. M.; Messersmith, P. B. Mussel-inspired surface chemistry for multifunctional coatings. *Science (80-.)*. **2007**, *318* (5849), 426–430.
- (10) Kang, S.; Elimelech, M. Bioinspired single bacterial cell force spectroscopy. *Langmuir* **2009**, *25* (17), 9656–9659.
- (11) Hutter, J. L.; Bechhoefer, J. Calibration of atomic-force microscope tips. *Rev. Sci. Instrum.* **1993**, *64* (7), 1868–1873.